High throughput microscopy of mechanism-based reporters in druginduced liver injury

Hiemstra, S.W.

Chapter 5

High content imaging-based comprehensive dynamic landscapes of oxidative stress response and DNA damage signaling during chemical exposure

Steven Hiemstra[1‡], Marije Niemeijer[1‡], Esmee Koedoot[1], Steven Wink[1], Janna Klip[1], Matthijs Vlasveld[1], Elisabeth de Zeeuw[1], Bram van Os[1], Andrew White[2] and Bob van de Water[1]

[‡]*Both authors contributed equally*

[1]Division of Toxicology, Leiden Academic Centre for Drug Research, Leiden University, Leiden, The Netherlands

[2]SEAC, Unilever, Colworth, United Kingdom

Manuscript in preparation

Abstract

A quantitative dynamics pathway map of Nrf2-mediated oxidative stress response and p53-related DNA damage response these pathways as well as the crosstalk between these pathways has not systematically been analysed. To allow the dynamic single cell evaluation of these pathways we have used BAC-GFP recombineering to tag for each pathway three key components: for the oxidative stress response, Keap1-GFP, Nrf2-GFP and Srxn1-GFP; for the DNA damage response, 53bp1-GFP, p53-GFP and p21-GFP. The dynamic activation of these individual components was mapped using quantitative high throughput confocal microscopy after treatment with a broad concentration range of diethyl maleate (DEM; to induce oxidative stress) and etoposide (to induce DNA damage). DEM caused a rapid activation of Nrf2, which returned to base line levels at low concentrations, but remained sustained at high concentration. Srxn1-GFP induction and KEAP1-GFP translocation to autophagosomes followed later, with upper boundaries reached at high concentrations, close to onset of cell death. Etoposide caused accumulation of 53BP1-GFP in DNA damage foci, which was later followed by the concentration dependent nuclear accumulation of p53-GFP followed by induction of p21-GFP. While etoposide caused activation of Nrf2-GFP and Srxn1-GFP, no activation of DNA damage reporters was observed for DEM. Interestingly, Nrf2 caused an inhibition of the DNA damage response at high concentrations of etoposide, while KEAP1 knock down caused an enhancement of the DNA damage response already at low concentrations of etoposide. Knock down of p53 did not affect the oxidative stress response. Altogether, the current stress response landscapes provide insight in the time course responses of and crosstalk between oxidative stress and DNA-damage and defines the tipping points where cell injury may switch from adaptation to injury.

Introduction

In the last decades, there is an urging need in the field of toxicology to develop new methods which assess toxicity pathways unraveling underlying mechanisms of toxicity[179]. The pivotal aspect in toxicity pathways is the balance between adaptation and cell death. Adaptive stress responses pathways allow the recovery from cell injury, thus re-establishing cellular homeostasis. However, when the stress is too severe, adaptive stress response pathways may reach there boundaries of activation prohibiting full recovery and provoking cell death as a consequence. Previously, we established a HepG2 BAC-GFP reporter platform to study the live cell dynamics of adaptive stress response pathway after cellular injury[145,180]. We tagged different signaling components of stress response pathways with green fluorescent protein (GFP), including the oxidative stress response and the DNA damage response, two critical pathways in chemical-induced injury. Both upstream regulators, critical pathway transcription factors and downstream target genes were tagged. By quantitatively assessing different components of the stress response pathways, we are now able to determine a detailed,

compound specific mode of action. Furthermore, the integration of these reporters with high throughput live cell imaging technologies allows the determination of the-point-of-departure and/or tipping point in concentration and time course experiments. This allows a full reflection of the cell physiological programs and is central in the assessment of the balance between adaptation and adversity [181]. In this study, we mapped in detail the landscape of the oxidative stress response and the DNA damage signaling pathways as well as their crosstalk.

Oxidative stress occurs when cells suffer from an increase in intracellular reactive oxygen species (ROS). ROS can damage proteins, nucleic acids and lipids [182]. Upon increase of intracellular concentrations of ROS, the anti-oxidant response pathway is activated by nuclear translocation of key transcription factor nuclear factor, erythroid 2-like 2 (*NFE2L2*/Nrf2) (Fig 1A). Under normal conditions, Nrf2 is bound by kelch-like ECH-associated protein 1 (Keap1) and targeted for proteasomal degradation through ubiquitination by Cul3[183]. Upon oxidative stress, ROS can modify cysteine residues of Keap1, thereby causing intracellular changes preventing the ubiquitination of Nrf2, and, thus, ensuring that all newly synthesized Nrf2 accumulates in the nucleus, where Nrf2 binds the anti-oxidant response element (ARE)[184]. This results in transcription of hundreds of target genes including detoxifying enzymes like Nqo1, Hmox1, Trx and Srxn1[185]. All together these targets ensure, amongst others, neutralization of ROS and cellular protection against oxidative stress.

The DNA Damage response (DDR) is activated after the induction of double stranded breaks (DSBs). DSBs can be caused by a wide range of agents including irradiation and chemicals. DSBs are sensed by proteins including MRN, ATM, ATR and DNA-PK. In order to transduce the signal, mediators 53bp1, MDC1 and BRCA1 locate to the DSBs at so-called DNA damage foci, and kinases CHK1 and CHK2 are activated. This leads to phosphorylation, stabilization and nuclear accumulation of tumor protein 53 (*TP53*/p53) and subsequent transcription of p53 targets. These targets include groups of genes which are responsible for cell cycle arrest (e.g. *CDKN1A*/p21), DNA repair and apoptosis (e.g. Bax and Puma) (Fig. 2A)[86].

Previous research showed contradictory links between the Nrf2 and p53 pathway signaling. Murine double minute 2 (Mdm2), a transcriptional target of p53, targets p53 for ubiquitination and proteasomal degradation serving as a negative feedback to restore homeostasis when DSBs are repaired[186]. Mdm2 is shown to be a target of Nrf2 in murine embryonic fibroblasts (MEFs) ovarian carcinoma A2780 and murine primary tubular epithelial cells[187,188]. This suggests that Nrf2 stimulation would lead to p53 down-regulation via Mdm2 up-regulation. In contrast, NAD(P)H:quinone oxidoreductase 1 (Nqo1), a transcriptional target of Nrf2, is proven to stabilize p53 during onset of oncogene-induced senescence in human diploid fibroblasts (HDF)[189]. A detailed assessment of crosstalk between these pathways has been limited due to the lack of dense concentration and time course experiments.

Here, using automated live cell high throughput confocal microscopy we followed single cell time dynamics of the oxidative stress response components (Keap1-GFP, Nrf2-GFP, Srxn1-GFP)

and the DNA damage signaling components (53bp1-GFP, p53-GFP and p21-GFP). We systematically assembled the concentration and time course landscapes for all six HepG2 BAC-GFP reporter cell lines after exposure of diethyl maleate (DEM) and etoposide. DEM is an electrophilic chemical, which alkylates the sulfhydryl group of glutathione and subsequently produces oxidative stress[190]. Etoposide inhibits DNA topoisomerase II activity. Topoisomerase II functions in DNA replication, transcription, DNA repair and chromatin remodeling. When topoisomerase II function is blocked by etoposide, DSBs will occur[191]. Crosstalk between these pathways was further investigated using RNA interference approaches.

Materials and Methods

Chemicals and antibodies

Etoposide and diethyl maleate (DEM) were purchased at Sigma (Zwijndrecht, the Netherlands). Compound stock solutions were made in dimethylsulfoxide (DMSO) from BioSolve (Valkenswaard, the Netherlands) and aliquots were stored at -20°C. The end concentration of solvent DMSO was equal or less than 0.2% (v/v). The antibody against GFP for Western Blot analysis was from Roche (Almere, the Netherlands). The antibody against tubulin was purchased at Sigma (Zwijndrecht, the Netherlands).

Cell culture

Human hepatocellular carcinoma HepG2 cell lines obtained from American Type Culture Collection (ATCC, Wesel, Germany) were cultured in Dulbecco's Modified Eagle Medium (DMEM) containing 10% (v/v) fetal bovine serum (FBS), 25 U/mL penicillin and 25 µg/mL streptomycin up until passage 20. Cells were cultured in a 5% CO_2 humidified incubator at 37°C.

RNA interference

Transient knock down of specific genes in HepG2 cells was achieved through reverse transfection of 50 nM siGENOME SMARTpool siRNAs from Dharmacon GE Healthcare (Eindhoven, the Netherlands) in combination with 0.3% INTERFERin transfection reagents from Polyplus (Leusden, the Netherlands). For the following genes transient knock down was performed, namely *KEAP1*, *NFE2L2* and *TP53*. As control, mock was used where no siRNA was added. Medium was refreshed 24 hours after transfection. Thereafter, the effect of knock down was evaluated 72 hours after transfection.

Confocal live cell imaging of HepG2 GFP reporters

To evaluate stress response activation, HepG2 BAC-GFP reporter cell lines for Keap1, Nrf2, Srxn1, 53bp1, p53 and p21 were established using bacterial artificial chromosome (BAC) recombineering as described previously[96,127,133,145]. To assess the effect of compound exposure on stress response activation, HepG2 GFP reporter cells were plated in µclear 384 wells plates

from Greiner Bio-One (Alphen aan den Rijn, the Netherlands). After attachment for 1 to 3 days, cells were stained for one hour with 100 ng/mL $Hoechst_{33342}$ and exposed to a broad concentration range of etoposide (0.001 - 100 µM) or diethyl maleate (0.01 - 1000 µM). As solvent control, cells were exposed to 0.2% DMSO. To evaluate the induction of cell death, medium also contained 0.05 % AnnexinV-Alexa633 and 100 nM propidium iodide (PI). The induction of GFP in the different reporters and cell death was examined through live cell automated confocal imaging for 24 hours after exposure using Nikon TiE2000 including an automated xy-stage, an integrated Perfect Focus System (Nikon, Amsterdam, the Netherlands) and 408, 488, 561 and 647 nm lasers.

Imaging data analysis

Quantification of the signal intensity was done using CellProfiler version 2.1.1 (Broad Institute, Cambridge, USA) with the modules as previously described[145]. For further analysis, the graphical user interface of the R package 'H5CellProfiler' (Wink *et al*., manuscript in preparation) and Rstudio (Boston, USA) was used to extract data of interest. For each imaging plate, the mean value of DMSO was calculated which resembled the background level. Thereafter, to determine the percentage of GFP positive cells, the fraction of cells which were three times above the background level was determined. Each replicate and each cell line was fitted with the b-spline method with 10 degrees of freedom, except for 53bp1 which was fitted with 3 degrees of freedom, and 3rd degree polynomials using the base-r lm and bs function from the splines R package to achieve resampling of the data with similar time points.

Western Blot analysis

Samples were collected by washing cells twice with cold 1x PBS and lysis with RIPA buffer containing freshly added 1% (v/v) cocktail protease inhibitors from Sigma (Zwijndrecht, the Netherlands). Cell lysate was spinned down at 13.000 rpm for 10 minutes at 4°C and supernatant was collected. To determine protein concentrations, BCA protein assay was performed. Thereafter, protein was dissolved with 1× sample buffer supplemented with 10 % v/v β-mercaptoethanol and heat-denatured at 95 °C for 5 min. After SDS-page protein separation, proteins were blotted onto PVDF membranes. Antibody incubations were performed in 1% BSA in TBS-0.05%Tween20. For detection, Pierce Enhanced Chemilumescent (ECL) Western Blotting substrate from Thermo Scientific (Bleiswijk, The Netherlands) was used and visualized using the ImageQuant LAS4000 from GE Healthcare (Eindhoven, the Netherlands).

Statistics

Results are shown as the mean ± the standard deviation from three biological replicates. Data analysis was done using GraphPad Prism 6.00 (GraphPad software, La Jolla, California, USA) and Rstudio (Boston, USA) using R 3.2.3 and the following R packages, namely ggplot2 (Wickham, 2015), data.table (Dowle *et al*, 2015), pheatmap (Kolde, 2015), reshape2 (Wickham, 2007), dplyr (Wickham and Francois, 2015), scales (Wickham, 2015), tidyr (Wickham, 2015), stats, splines and graphics. Significance levels were calculated using Student's t-test, *p < 0.05, **p < 0.01, ***p < 0.001.

Results

High content live cell imaging of oxidative stress and DNA damage HepG2 GFP reporters.

To evaluate the Nrf2 anti-oxidant response pathway and the p53 DNA damage repair pathway in detail, different components of the pathways were imaged after administration of two known inducers of oxidative stress (DEM) and DNA damage (etoposide). For both stress pathways an upstream sensor, a transcription factor and a specific transcriptional target were chosen (supplemental figure 1). For the Nrf2 anti-oxidant pathway, Keap1 was chosen as a sensor, Nrf2 as the transcription factor and Sulfiredoxin1 (Srxn1) as the specific downstream target of Nrf2. For the p53 DNA damage repair pathway, p53 binding protein 1 (53bp1) was chosen as a sensor, p53 as the transcription factor and $p21^{CIP1/WAF1}$ as the specific downstream target of p53. These six GFP reporters were seeded in a high content 384 well format and subsequently exposed to a broad dose range of DEM (from 10 nM to 1 mM) and etoposide (1 nM to 100 µM). Live cell confocal imaging allowed single cell image analysis to identify GFP intensity in the cytoplasm (Srxn1-GFP) and nucleus (Nrf2-GFP, p53-GFP and p21-GFP) and cytoplasmic and nuclear foci count (Keap1-GFP, 53bp1-GFP) (supplemental figure 1).

Nrf2 pathway activation after administration to DEM showed a time and concentration dependent increase for each component of the pathway (figure 1B and D). With increasing concentrations of DEM, increased pathway activation was observed. However, concentrations above 316 µM led to a reduction in Srxn1-GFP and Keap1-GFP activation; this was associated with the onset of cell death (supplemental figure 2). At 1 mM DEM a sustained nuclear accumulation of Nrf2-GFP was observed, while simultaneously Srxn1-GFP accumulation did not reach its maximal activation, indicating that Nrf2 was highly activated, but was not able to switch to the adaptive program. To assess the single cell time dynamics of transcriptional activity of Nrf2, Srxn1-GFP cytoplasmic intensity was evaluated. Exposure to 100 µM DEM led to a small increase in Srxn1-GFP intensity after 2 hours, which further increased until 24 hours. A small population of Srxn1-GFP cells were high responders, which had about two to three times higher GFP intensity (figure 1C, left panel). This is also visible in the histogram where the amount of cells are listed against GFP intensity after 12,5 hours of 100 µM DEM (figure 1C, right panel). The broad concentration range allowed us to define the point of departure (PoD) concentration. Therefore, we defined this concentration for GFP intensity, fraction positive cells

and AUC values for each reporter (table 1). The PoD of Srxn1-GFP was ~10-fold lower than PoD of Keap1-GFP and Nrf2-GFP. This seems counterintuitive as Nrf2 and Keap1 first need to be activated before Srxn1 can be produced. A likely explanation is the sensitivity of the reporters, as Srxn1-GFP exhibits higher levels of GFP signal.

Etoposide administration led to a robust concentration and time dependent increase of p53-GFP and p21-GFP (figure 1B and 1D). 53bp1-GFP foci count showed a dose dependent effect in percentage GFP positive cells and area under the curve (AUC) of the time curves. However, at 1 and 10 µM etoposide a time dependent activation was not observed. Single cell p21-GFP intensities resulted in larger variation compared to Srxn1-GFP (figure 1C and 2C left panels). This was due to a larger population of high responding p21-GFP cells. This was also observable

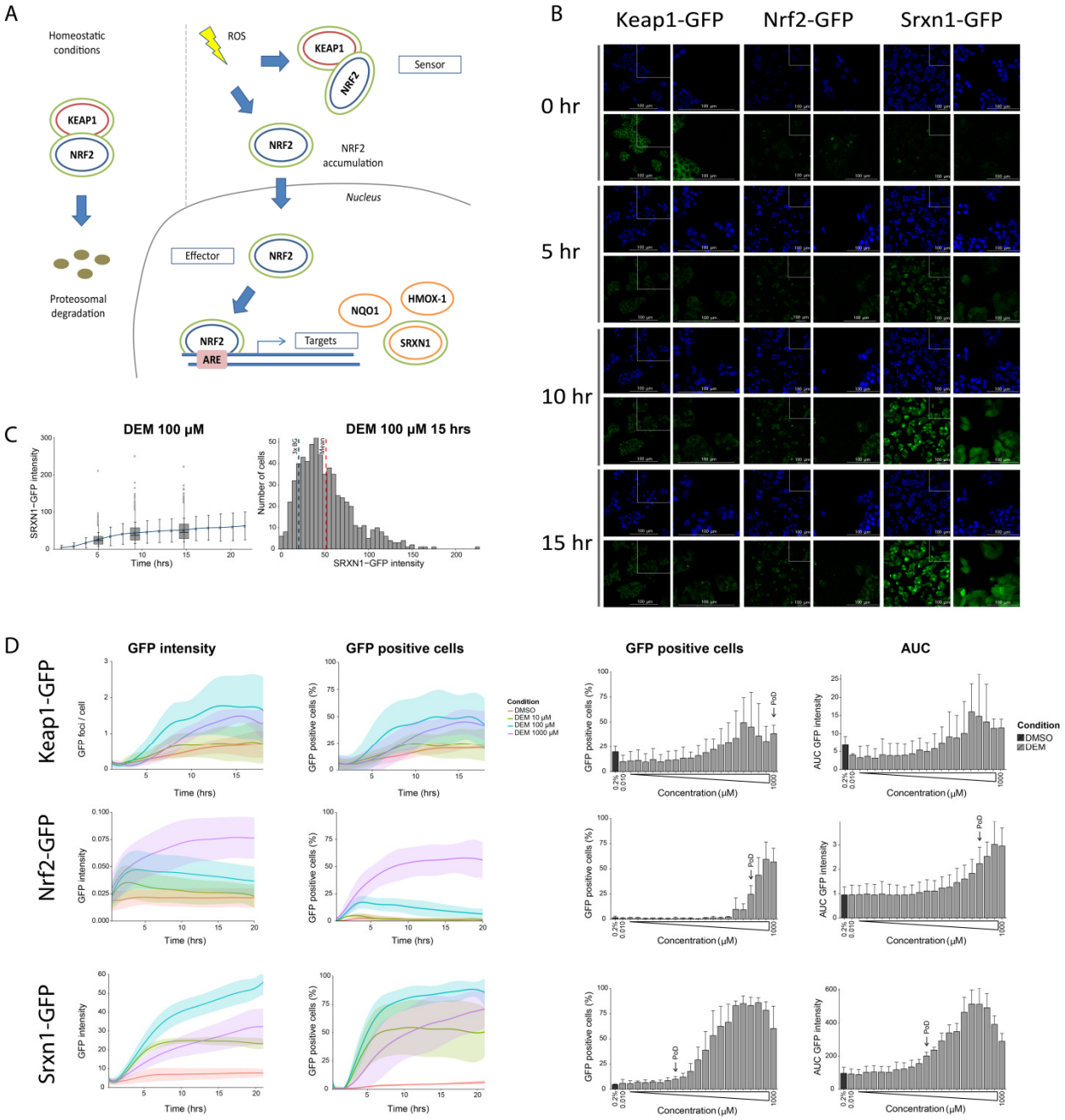

Figure 1: Imaging based Nrf2 anti-oxidant pathway response to diethyl maleate (DEM). A) Nrf2 pathway regulation. In normal conditions the Keap1-Nrf2 complex is degraded. Under ROS conditions, Nrf2 accumulates and translocates to the nucleus. Nrf2 binds the anti-oxidant respons element (ARE) and transcribes it's targets. Pathway components indicated with a green circle are tagged with Green Fluorescent Protein (GFP). B) Example images of 100 µM DEM for 0, 5, 11 and 17 hours after exposure. One time point consists of four images per reporter, an overview image of nuclear staining (upper left image), an overview image of GFP (lower left image), a zoom image of nuclear staining (upper right image) and a zoom image of GFP (lower right image). C) Variation in Srxn1-GFP of one replicate experiment, plotted as GFP intensity over time including standard deviation and boxplots to display the variation (left panel) and plotted as a histogram displaying number of cells over GFP intensity including blue bar to indicate three times background levels and red bar indicating the mean GFP intensity (right panel). D) DEM responses of Keap1-GFP, Nrf2-GFP and Srxn1-GFP, shown in four graphs per reporter. GFP foci count (Keap1) and GFP intensity (Srxn1 and Nrf2) over time for DMSO, 10 µM, 100 µM and 1000 µM DEM (upper left), fraction GFP positive cells over time for DMSO, 10 µM, 100 µM and 1000 µM DEM (upper right), GFP foci count (Keap1) and GFP intensity (Srxn1 and Nrf2) displayed in dose response (lower left) and area under the curve (AUC) of GFP foci count (Keap1) and GFP intensity (Srxn1 and Nrf2) time responses displayed in dose response (lower right). Standard deviations are shown for three independent

in the amount of cells per GFP intensity group (figure 2C, right panel). PoD evaluation led to a lower PoD of 53bp1-GFP, compared to p53-GFP and p21-GFP (table 1). This indicates that 53bp1 foci formation already occurs at lower concentrations, without full p53 pathway activation. Pathway activation was verified by measuring p21-GFP protein levels by Western Blotting (supplemental figure 2).

		DEM		Etoposide	
Pathway		% positive cells	AUC	% positive cells	AUC
Oxidative stress	Keap1-GFP	1000 µM	NS	NS	NS
	Nrf2-GFP	178 µM	178 µM	NS	NS
	Srxn1-GFP	0.563 µM	3.16 µM	17.8 µM	10 µM
DNA damage response	53bp1-GFP	NS	NS	0.56 µM	0.56 µM
	p53-GFP	178 µM	NS	1.0 µM	5.6 µM
	p21-GFP	316 µM	178 µM	3.2 µM	3.2 µM

Table 1: Point of departure (PoD) concentrations of p53 and Nrf2 signaling GFP reporters exposed to DEM and etoposide. Point of departure concentration for Keap1-GFP, Nrf2-GFP, Srxn1-GFP, 53bp1-GFP, p53-GFP and p21-GFP as percentage cells exceeding two times background and area under the curve (AUC) of 24 hour time courses in response to diethyl maleate (DEM) and etoposide. All concentrations are in µM, NA is not available.

High concentrations of etoposide and DEM activate Srxn1-GFP and p21-GFP respectively

Next we examined possible crosstalk between the protective Nrf2 pathway and the p53 pathway. We focused on the Srxn1-GFP and p21-GFP, respectively, since they represent the

entire pathway activation and are most sensitive, allowing most accurate overall pathway activity. The PoD concentration of Srxn1-GFP exposed with etoposide was 5.6 µM; at 100 µM etoposide, more than 75% of the cells were positive for Srxn1-GFP (two times higher GFP intensity than background levels; figure 3A and B). Thus etoposide can activate the Nrf2 response, but is much less potent than DEM. Similarly, we determined the effect of DEM on p21-GFP activation. The PoD of p21-GFP exposed to DEM was 178 µM; in addition,1000 µM DEM was a less potent inducer of p21-GFP than 100 µM etoposide of Srxn1-GFP, as only 25% of p21-GFP cells were counted as GFP positive, with an overall intensity which was four times lower than for p21-GFP cells exposed to etoposide. Despite, a clear activation of p21-GFP was observable. In conclusion, cross activation with two known inducers was present in HepG2 cells, however, especially in DEM-induced p21-GFP activation, the activation was much less potent

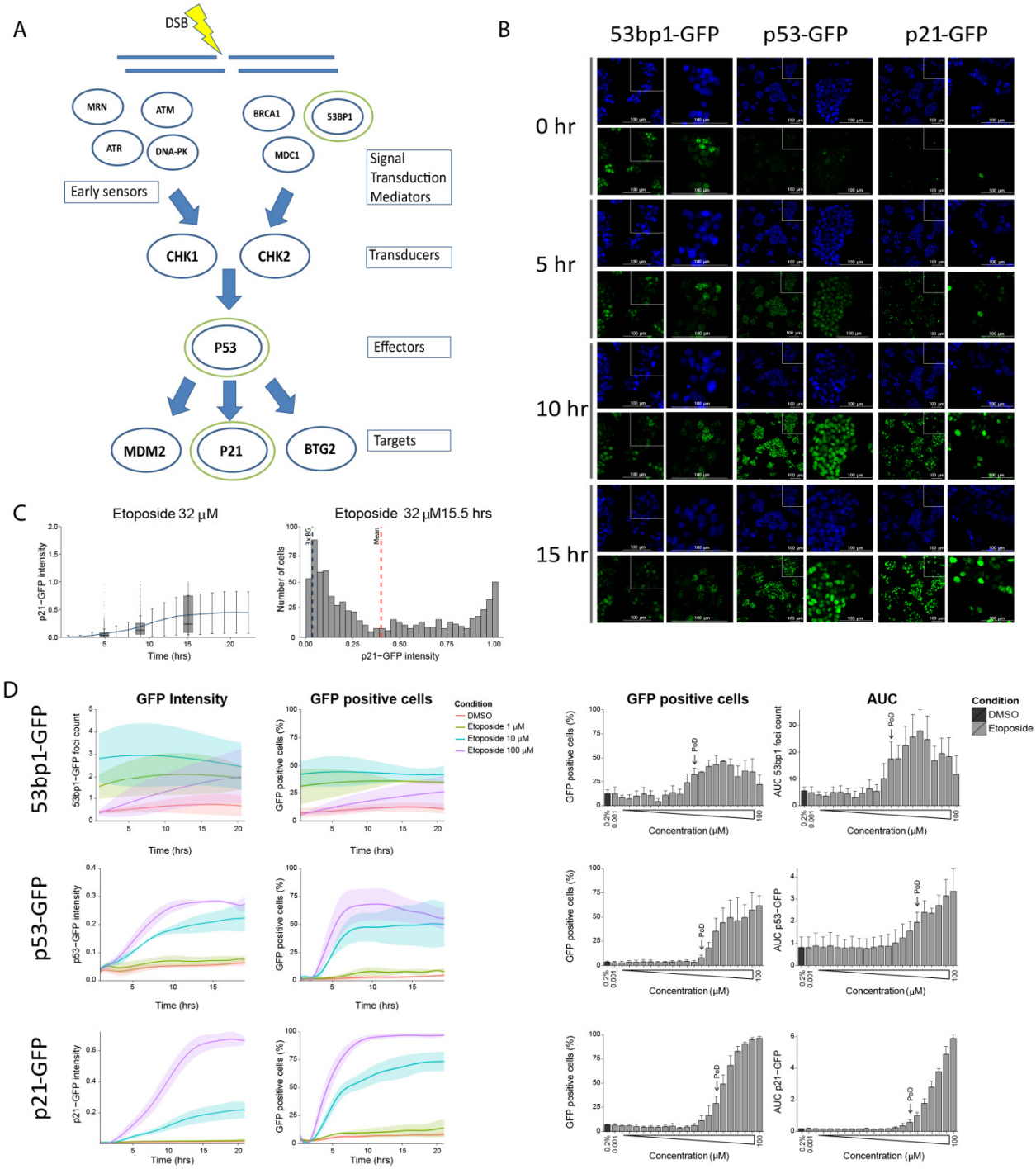

Figure 2: p53 DNA damage pathway response to etoposide. A) p53 pathway regulation. Double stranded breaks (DSBs) in the DNA are sensed by proteins including MRN, ATM, ATR and DNA-PKs. Adaptor/mediator proteins including BRCA1, MDC1 and 53bp1 transduce the signal to CHK1 and CHK2, which subsequently activate p53. p53 accumulates in the nucleus and transcribes targets as p21, Btg2 and Mdm2. Pathway components indicated with a green circle are tagged with Green Fluorescent Protein (GFP). B) Example images of 31,6 µM etoposide for 0, 5, 11 and 17 hours after exposure. One time point consists of four images for each reporter, an overview image of nuclear staining (upper left image), an overview image of GFP (lower left image), a zoom image of nuclear staining (upper right image) and a zoom image of GFP (lower right image). C) Variation in p21-GFP of one replicate experiment, plotted as GFP intensity over time including standard deviation and boxplots to display the variation (left panel) and plotted as a histogram displaying number of cells over GFP intensity including blue bar to indicate three times background levels and red bar indicating the mean GFP intensity (right panel). D) Etoposide responses of 53bp1-GFP, p53-GFP and p21-GFP, shown in four graphs per reporter. GFP foci count (53bp1) and GFP intensity (p21 and p53) over time for DMSO, 1 µM, 10 µM and 100 µM etoposide (upper left), fraction GFP positive cells over time for DMSO, 1 µM, 10 µM and 100 µM etoposide (upper right), GFP foci count (53bp1) and GFP intensity (p21 and p53) displayed in dose response (lower left) and area under the curve (AUC) of GFP foci count (53bp1) and GFP intensity (p21 and p53) time responses displayed in dose response (lower right). Standard deviations are shown for three independent replicates.

(table 1), indicating specificity of stress response pathway activation by DEM, and limited crosstalk. On the contrary, etoposide did induce more potent crosstalk with the Nrf2 signaling pathway.

Knock down of KEAP1 causes an increase of p21-GFP

Since activation of p21-GFP by DEM and Srxn1-GFP by etoposide was observed at higher concentrations, secondary mode of actions of these compounds could play a role. For example, ROS induced by high concentrations of DEM could also affect nucleic acids and induce DSBs activating the p53 pathway. To eliminate the possibility of such secondary effects of the chemicals, knock down experiments were conducted. Srxn1-GFP and p21-GFP levels were measured after knock down of *KEAP1*, *NFE2L2* and *TP53*. Knock down of *KEAP1* resulted in significantly higher levels of Srxn1-GFP without stimulation with DEM (figure 4A and B). As expected, knock down of *NFE2L2* led to significantly lower Srxn1-GFP levels after induction with DEM. This holds true for both 10 and 100 µM DEM exposures. 1000 µM of DEM showed a similar trend, however the presence of higher levels of cell death increased possibly the variation. Knock down of *TP53* resulted in a decrease in Srxn1-GFP compared to mock control situation, however this difference was only significant in 10 µM DEM after 21 hours of exposure. This decrease may suggest that the upregulation of Srxn1 after etoposide is at least partly due to direct biological communication between the p53 and the Nrf2 pathway.

As expected, knock down of *TP53* led to an almost complete prevention of the induction of p21-GFP after exposure to etoposide (figure 4C and D). *NFE2L2* knock down did not affect p21-

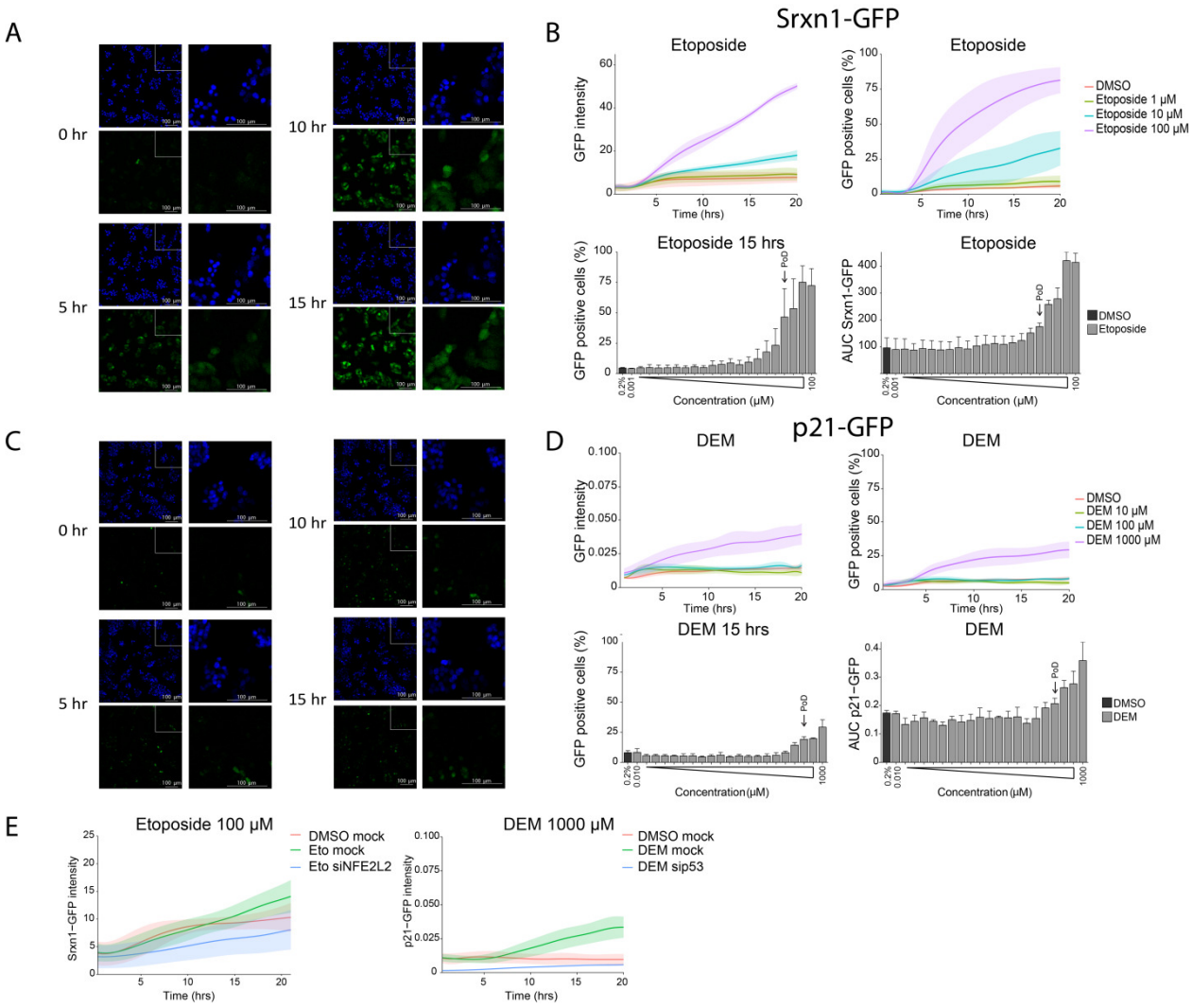

Figure 3: Crosstalk between oxidative stress and DNA damage only occurs at high concentrations of etoposide and DEM respectively. A) Example images of Srxn1-GFP exposed to 31,6 µM etoposide for 0, 5, 11 and 17 hours. One time point consists of four images for each reporter, an overview image of nuclear staining (upper left image), an overview image of GFP (lower left image), a zoom image of nuclear staining (upper right image) and a zoom image of GFP (lower right image). B) Etoposide responses of Srxn1-GFP, shown in four graphs: GFP intensity over time for DMSO, 1 µM, 10 µM and 100 µM etoposide (upper left), fraction GFP positive cells over time for DMSO, 1 µM, 10 µM and 100 µM etoposide (upper right), GFP intensity displayed in dose response (lower left) and area under the curve (AUC) of GFP intensity time responses displayed in dose response (lower right). Standard deviations are shown for three independent replicates. C) Example images of p21-GFP exposed to 100 µM DEM for 0, 5, 11 and 17 hours. One time point consists of four images for each reporter, an overview image of nuclear staining (upper left image), an overview image of GFP (lower left image), a zoom image of nuclear staining (upper right image) and a zoom image of GFP (lower right image). D) DEM responses of p21-GFP, shown in four graphs: GFP intensity over time for DMSO, 10 µM, 100 µM and 1000 µM DEM (upper left), fraction GFP positive cells over time for DMSO, 10 µM, 100 µM and 1000 µM DEM (upper right), GFP intensity displayed in dose response (lower left) and area under the curve (AUC) of GFP intensity time responses displayed in dose response (lower right). Standard deviations are shown for three independent replicates.

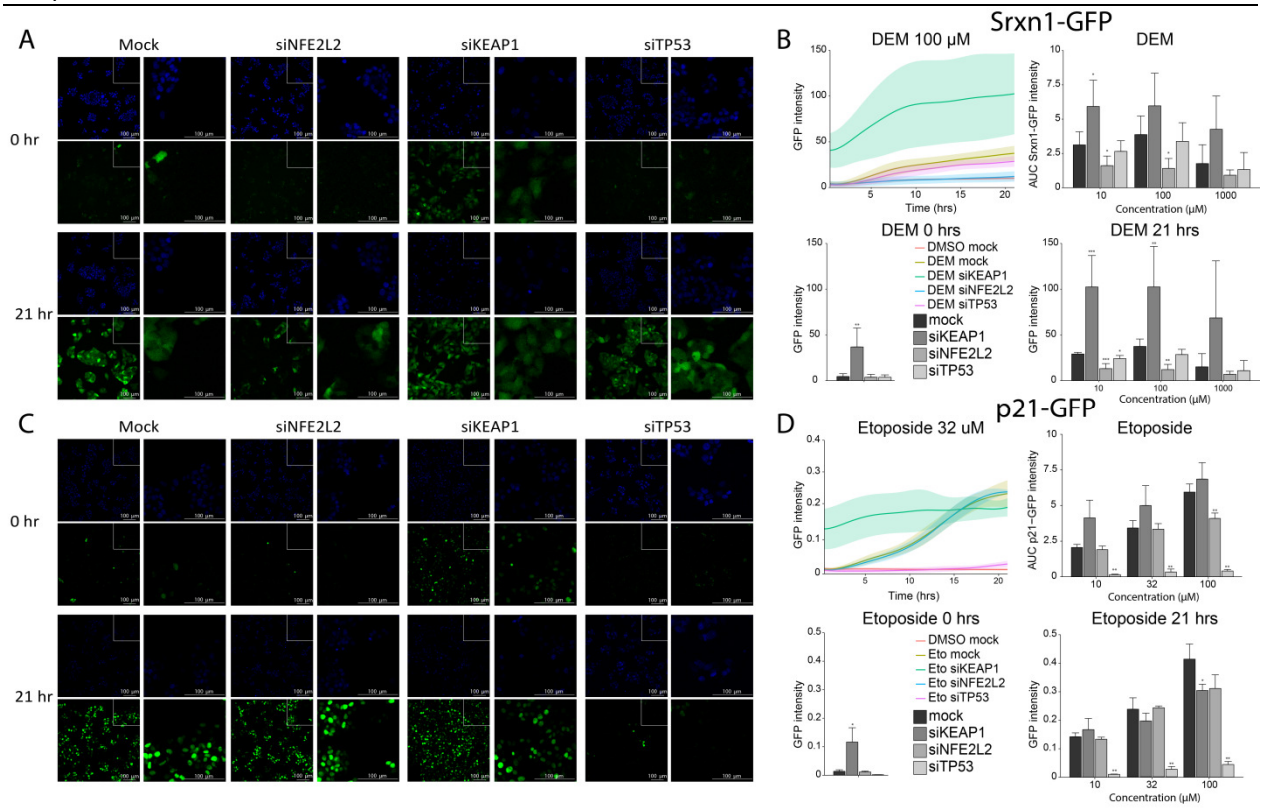

Figure 4: Knock down of *KEAP1*, *NFE2L2* and *TP53* in Srxn1-GFP and p21-GFP. A) Example images of Srxn1-GFP without knock down (mock) and with knock down (*siNFE2L2, siKEAP1* and *siTP53*) with exposure to 100 µM DEM for 0 and 21 hours. One time point consists of four images for each reporter, an overview image of nuclear staining (upper left image), an overview image of GFP (lower left image), a zoom image of nuclear staining (upper right image) and a zoom image of GFP (lower right image). B) DEM responses of Srxn1-GFP, shown in four graphs: GFP intensity over time for mock, *siKEAP1*, *siNFE2L2* and *siTP53* after exposure to 100 µM DEM (upper left), area under the curves of GFP time response after exposure to 10 µM, 100 µM and 1000 µM DEM (upper right), GFP intensity displayed for 0 hours of DEM exposure after mock and *siKEAP1, siNFE2L2* and *siTP53* (lower left) GFP intensity displayed for 21 hours of DEM exposure after mock and *siKEAP1, siNFE2L2* and *siTP53* (lower right). Standard deviations are shown for three independent replicates. Significance (* = $p < 0.05$, ** = $p < 0.01$) calculated with a one-tailed Student's t-test for 0 hours DEM and a two-tailed Student's t-test for AUC and 21 hours DEM. C) Example images of p21-GFP without knock down (mock) and with knock down (*siNFE2L2, siKEAP1* and *siTP53*) with exposure to 31,6 µM etoposide for 0 and 21 hours. One time point consists of four images for each reporter, an overview image of nuclear staining (upper left image), an overview image of GFP (lower left image), a zoom image of nuclear staining (upper right image) and a zoom image of GFP (lower right image). D) Etoposide responses of p21-GFP, shown in four graphs: GFP intensity over time for mock, *siKEAP1*, *siNFE2L2* and *siTP53* after exposure to 31,6 µM etoposide (upper left), area under the curves of GFP time response after exposure to 1 µM, 10 µM and 100 µM etoposide (upper right), GFP intensity displayed for 0 hours of etoposide exposure after mock and *siKEAP1, siNFE2L2* and *siTP53* (lower left) GFP intensity displayed for 21 hours of etoposide exposure after mock and *siKEAP1, siNFE2L2* and *siTP53* (lower right). Standard deviations are shown for three independent replicates. Significance (* = $p < 0.05$, ** = $p < 0.01$) calculated with a one-tailed Student's t-test for 0 hours etoposide and a two-tailed Student's t-test for AUC and 21 hours etoposide.

GFP levels after etoposide treatment. Interestingly, p21-GFP was significantly upregulated after knock down of *KEAP1*.

KEAP1 knock down causes upregulation of different components of both the Nrf2 and the p53 pathway.

The above studies suggest a direct interaction between the Nrf2 and the p53 pathway, whereby *KEAP1* knock down stimulates the p53 pathway. To assess this central role of Keap1 in further detail, we first performed knock down in additional GFP reporter cell lines. Previous observations in this area described Nqo1 and Mdm2 as important players as a bridge between the Nrf2 and p53 pathway[186,188,189], for that reason Nqo1-GFP and Mdm2-GFP reporters were used as an additional read-out. In addition, we tested p53-GFP reporter as an additional component of the p53 pathway. First, we validated knock down of *KEAP1* in two targets of Nrf2: Srxn1-GFP and Nqo1-GFP. Both showed significant upregulation ensuring these reporters are Keap1 regulated (figure 5B). Next, we tested knock down of Keap1 in DNA damage components p53-GFP, p21-GFP and Mdm2-GFP. Again, Keap1 knock down demonstrated significant upregulation of p21-GFP, as well as p53-GFP. Mdm2-GFP was not affected by Keap1 knock down (figure 5B). This suggests a role for Keap1 in the p53-p21 axis. To identify whether this role was Nrf2 dependent, a double knock down of Keap1 and Nrf2 was performed for p21-GFP and p53-GFP. The double knock down did not result to a significant increase in p21-GFP, however it did in p53-GFP (figure 5B). In both p21-GFP and p53-GFP double knock down showed less induction compared to knock down of Keap1 alone, suggesting Nrf2 dependency. Whether this is the case and whether this Nrf2 dependency is regulated via Nqo1 needs to be elucidated in future studies.

Discussion

Chemical exposure can lead to cellular injury and activation of adaptive stress response pathways. Little is known on the dynamics of these pathways and on how these pathways are integrated and controlled by similar key events and signaling components. Therefore, it is essential to map the dynamics of the activation of adaptive stress responses and their intracellular relationship, such as the oxidative and DNA damage stress response. Using a HepG2 GFP reporter panel specific for oxidative and DNA damage stress signaling in combination with live cell high-content confocal imaging concentration and time-dependent activation of Nrf2 and p53 pathway components by relevant reference compounds could be observed. Reference compounds, DEM and etoposide, could activate Nrf2 and p53 signaling, respectively. By treating in a broad range of concentrations, the concentration from where the response is first observed, the point of departure (PoD), could be determined accurately. In addition, etoposide did also activate the Nrf2 pathway, while DEM could activate p53 pathway, albeit both at higher PoD concentrations. This suggest cross signaling between these stress

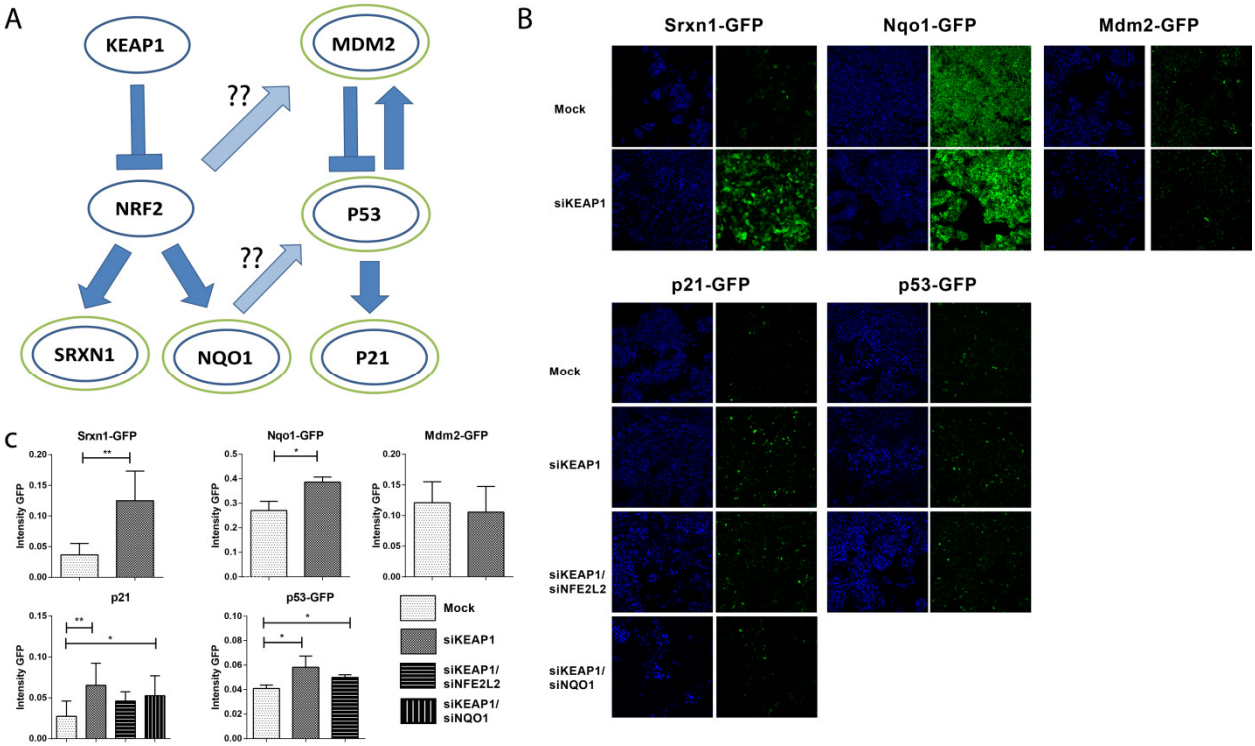

Figure 5: Knock down of *KEAP1* in Srxn1-GFP, p21-GFP, Nqo1-GFP, Mdm2-GFP and p53-GFP. A) Possible crosstalk mechanism between Nrf2 and p53 pathway. Pathway components indicated with a green circle are tagged with Green Fluorescent Protein (GFP). B) Knock down of *KEAP1* for Srxn1-GFP, Nqo1-GFP, Mdm2-GFP, p21-GFP and p53-GFP compared to the mock condition. Double with *KEAP1* and *NFE2L2* for p21-GFP and p53-GFP. Standard deviations are shown for three independent replicates. Significance (* = $p < 0,05$, ** = $p < 0,01$) calculated with a one-tailed Student's t-test.

response pathways, in particular when chemical insult is more severe. Interestingly, loss of Keap1 function by siRNA knock down led to an increase in basal p53 pathway activation, suggesting direct interaction between Nrf2 signaling and DNA damage response. Overall, our current data provide comprehensive maps of two adaptive stress response pathways that are critical in chemical-induced injury illustrating the strength of our reporter systems in high content imaging analysis of stress pathway activation.

DEM led to increased levels of Keap1 foci, Nrf2 and Srxn1 in HepG2 reporter cells over time. Upon oxidative stress, Keap1 is no longer able to target Nrf2 for proteasomal degradation[183]. First, Keap1 is bound by p62 and targeted for degradation[192]; second, Nrf2 accumulates in the nucleus and third, Srxn1 and other Nrf2 targets are upregulated. Our observed time-dynamics of the Nrf2 response activation by DEM revealed initial rapid Nrf2 induction, within 1 hour with a maximum at ~4 hours, followed by a late, >4 hours, and sustained onset of Keap1 foci formation. It has been suggested that Keap1 turnover is mainly governed by autophagy in a p62-dependent manner[193]. Indeed, Keap1-GFP foci co-localize with p62 (data not shown). Importantly, Nrf2 directly activates the expression of Keap1 as well as p62[185]. Thus, upon Nrf2 stimulation, all newly assembled Keap1 cannot bind to Nrf2 and will bind to p62 instead. Thus, our late Keap1 foci formation is likely rather a consequence than a cause of Nrf2 activation.

These findings exemplify the explicit enhanced information of a quantitative imaging-based analysis of the dynamic behavior of individual Nrf2 signaling components.

Regarding the time dynamics of the DNA damage response, exposure to model compound etoposide led to the almost immediate formation of 53bp1 DNA damage foci, within ~3 hours followed by p53 upregulation and almost direct subsequent increased levels of p21. Despite the clear increase in 53bp1-GFP foci, a considerable variation in number of 53bp1 foci between the replicates was observed during exposure to etoposide. This is possibly due to higher zoom used for image acquisition to allow sufficient resolution of foci detection, but consequently each image contained less cells. In addition, due to the longer image acquisition time, the time resolution was ~2.5 hours, which limited the more detailed analysis of the entire foci dynamics. A fast 53bp1 foci formation response with a peak at 1 hour post etoposide exposure was reported in HeLa cells[194] and for irradiation, 20 minutes was the maximal 53bp1 response[195]. Therefore, due ot our imaging limitations we might have missed the steep initial dynamics of 53bp1 foci formation at the lower concentrations of etoposide. Intriguingly, the highest concentration of etoposide showed a gradual and sustained increase of 53bp1 foci for the entire 24 hours period exposure; possibly this high concentration affects the effectiveness of the DNA damage recognition programs and prohibits the rapid association of 53bp1 at DNA damage sites. Yet, this reduced 53bp1 accumulation was not reflected by an inhibition of p53-GFP stabilization and reduced p21-GFP induction. This suggest that there does not seem to be a direct quantitatively relationship between foci number and p53 activity. Future studies should elucidate the mechanism of reduced foci formation at high concentrations of etoposide.

The broad concentration range of DEM and etoposide allowed precise identification of the PoD for each pathway component. PoD identification revealed a specific pathway response: DEM showed a much lower PoD for Nrf2 activation (1.8 µM) than for p53 activation (178 µM); yet, etoposide demonstrated a PoD for Nrf2 activation (5.6 µM) that was close to the PoD of p53 activation (1.0 µM). These results suggest crosstalk as DEM and etoposide can activate p53 and Nrf2 signaling respectively. Although we have not measured the actual effect of DEM on cellular glutathione homeostasis, we suspect that at the lower levels no major glutathione decrease has occurred, and that the Nrf2 activation is directly mediated by modulation of cysteine residues of Keap1. At the higher concentration glutathione might become decreased, allowing the onset of oxidative stress and thereby initiation of ROS mediated DNA damage, which is detected by the p53 pathway. The fact that or etoposide the PoD for p53 and Nrf2 activation are so close, suggests a similar molecular initiation events, i.e. the DNA damage, causes activation of both program, albeit that the etoposide-induced Nrf2 activation does not parallel the efficiency and amplitude as observed for DEM.

Depletion of Keap1 due RNA interference resulted in an increase of basal p53 and p21 activation levels, suggesting either a direct inhibitory role of Keap1 on the DNA damage response. Atlernatively Keap1 has an indirect role through inhibition of the Nrf2, and thus,

increased Nrf2 activity would promote the p53-mediated induction of p21 expression. Indeed, double knock down of Keap1 and Nrf2 resulted in a partial restoration of p21 and p53 basal levels, thus pointing to additional mechanisms. Recently, Nrf2-induced Nqo1 was shown to promote p53 accumulation during oncogene-induced senescence which was Mdm2 independent [189]. As expected, downregulation of Keap1 resulted in significant higher levels of Nqo1, a bona fide Nrf2 target gene. As such, upregulation of Nqo1 after Keap1 knock down could than modulate p53 levels, followed by p21 upregulation. Regarding the crosstalk between p53 signaling and the Nrf2 pathway, it is noteworthy that p21 can bind the DLG and ETGE motifs of Nrf2 and thereby competing with Keap1 for Nrf2 binding; the p21 binding leads to enhanced accumulation of Nrf2[196]. Possibly the etoposide-induced Nrf2 activation is partly related to this p21-mediated Nrf2 stabilization effect.

Here, we utilized our established HepG2 GFP reporters to provide a detailed mapping of the dynamics landscape of the oxidative stress response and DNA damage signaling pathways. We recognize that the components used are ownly a reflection of the complexity of the entire pathways. Regardless, the current reporters provide an overall high level detail on the dynamics of several key components. We feel that these detailed quantitative landscapes are fit-for-purpose to define PoD for pathway activation as well as possible crosstalk. In addition, this data can be used for mathematical modeling to assess detailed information on pathway regulation in response to adaptive stress response activation. Future directions will involve integration of multiple adaptive stress response reporters in one cell line to closely follow the dynamics of individual stress response pathway components at the single cell level and unravel their synchronized timing of activation at their variations at the population level.

Acknowledgements

This work was supported by a Unilever SEAC research grant, the IMI MIP DILI project (grant agreement number 115336) and the EU FP7 Seurat-1 Detective project (grant agreement number 266838).

Supplementals

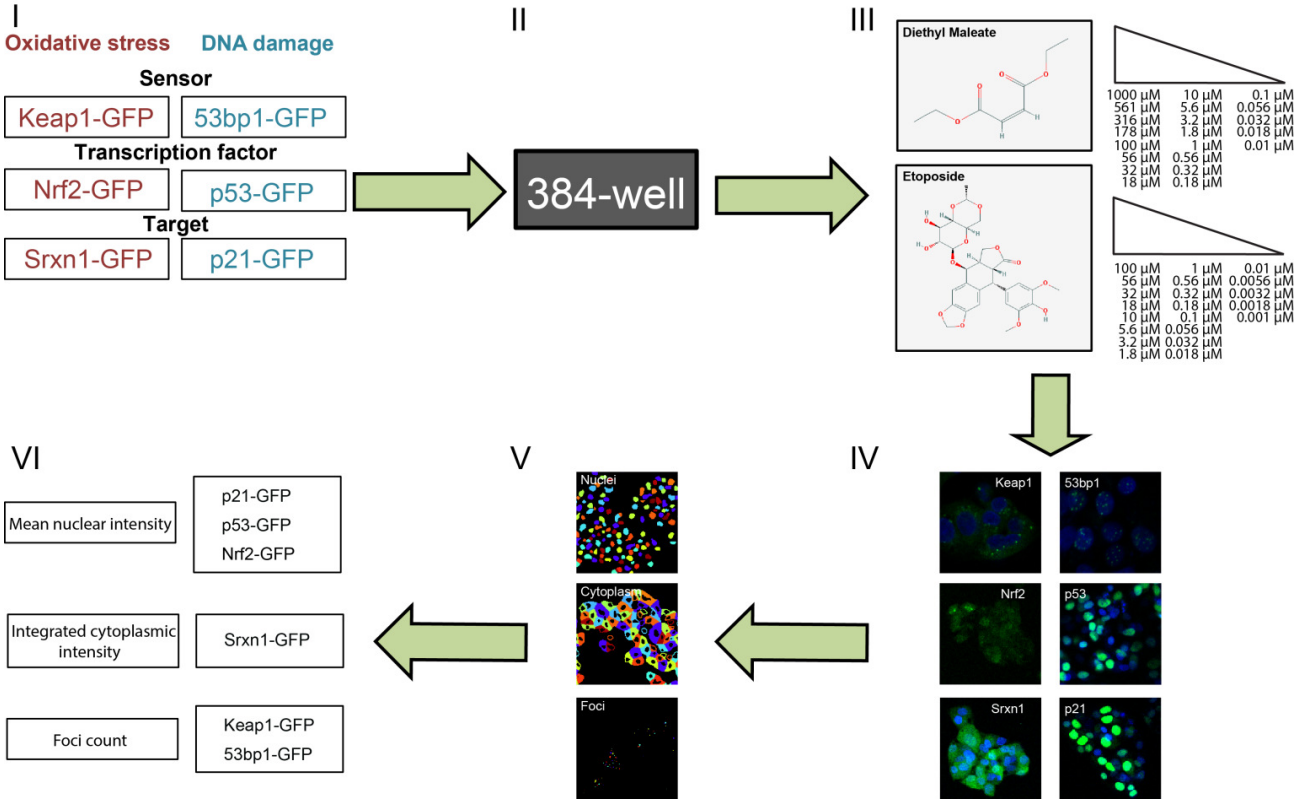

Supplemental figure 1: Workflow of GFP reporter exposure, image acquisition and image analysis. I) Three GFP reporters of both Nrf2 and p53 pathway are II) seeded in a 384-well format, III) exposed to a broad dose range of model compounds diethylmaleate and etoposide followed by IV) image acquisition, V) image analysis and VI) GFP read-out.

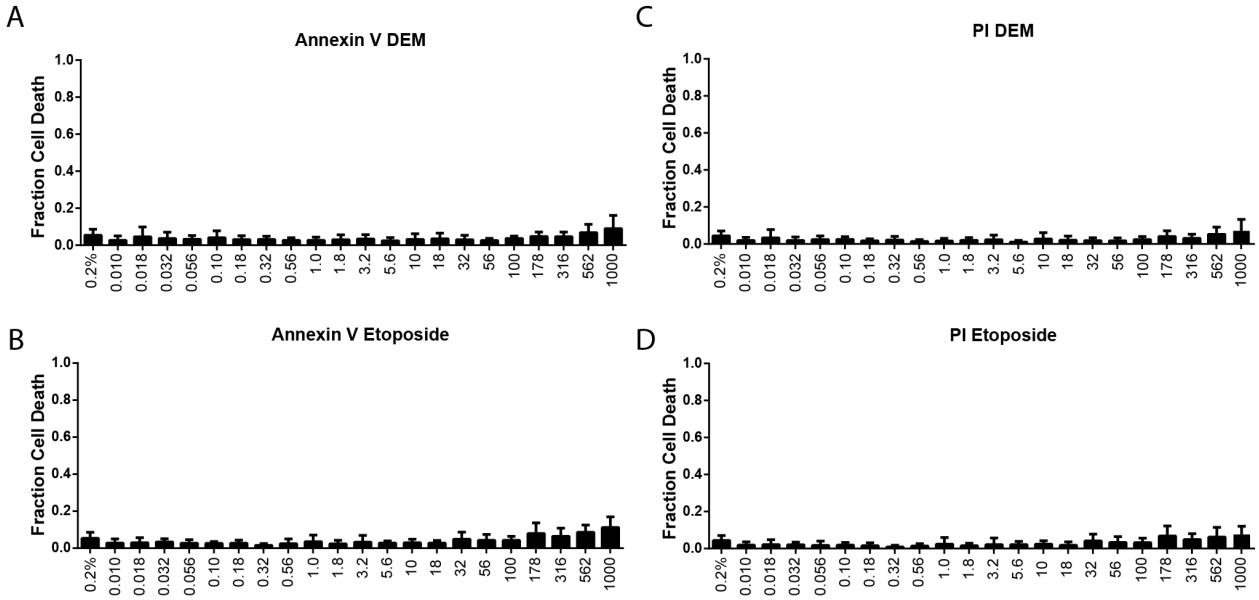

Supplemental figure 2: Cell death markers for DEM and etoposide. A) AnnexinV in fraction positive cells for 0.2% DMSO and 21 concentrations of DEM. B) Propidium iodide (PI) in fraction positive cells for 0.2% DMSO and 21 concentrations of DEM C) AnnexinV in fraction positive cells for 0.2% DMSO and 21 concentrations of etoposide. D) Propidium iodide (PI) in fraction positive cells for 0.2% DMSO and 21 concentrations of etoposide. Mean and standard deviation shown for three replicates of reporters Nrf2-GFP, Srxn1-GFP, p21-GFP and p53-GFP.

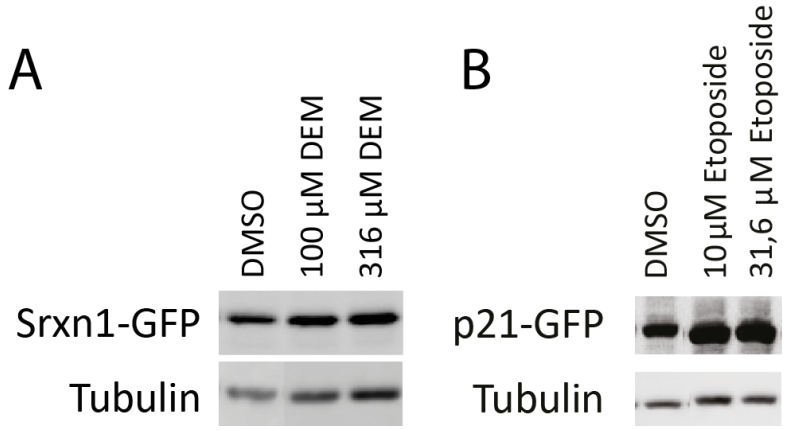

Supplemental figure 3: Western blot analysis of Srxn1-GFP and p21-GFP after DEM and etoposide exposure respectively. A) Western blotting with the GFP antibody in Srxn1-GFP cells exposed to DMSO (0.2%), 100 µM and 316 µM DEM. B) Western blotting with the GFP antibody in p21-GFP cells exposed to DMSO (0.2%), 10 µM and 31.6 µM etoposide.

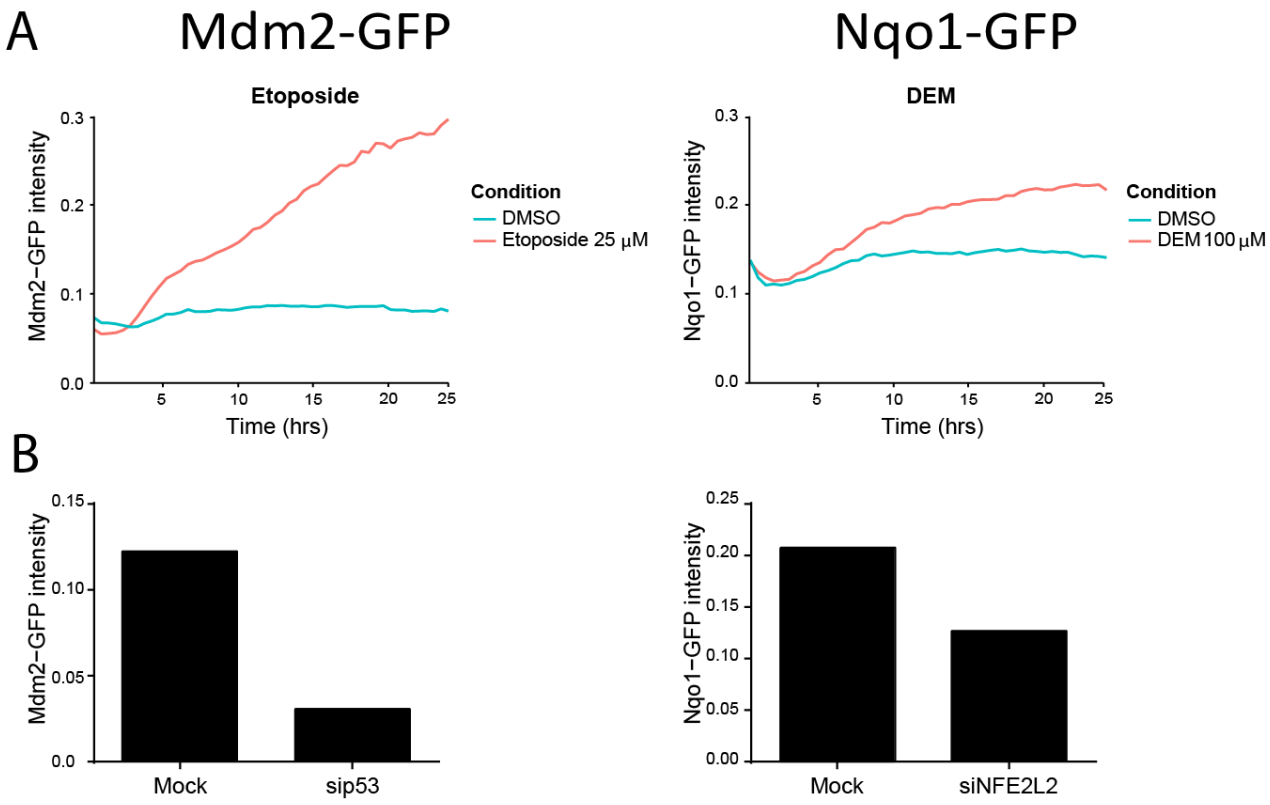

Supplemental figure 4: Live cell dynamics of Mdm2-GFP and Nqo1-GFP. A) Mdm2-GFP stimulated with 25 µM etoposide and monitored for 24 hours live cell imaging (left graph) and Nqo1-GFP stimulated with 100 µM DEM (right graph). B) Mdm2-GFP intensity after 24 hours of stimulation with etoposide for untransfected control mock and sip53 (left graph) and Nqo1-GFP intensity after 24 hours of stimulation with DEM for untransfected control and siNFE2L2.